



Citation for published version:

Leong, SX, Carta, M, Malpass-evans, R, Mckeown, NB, Madrid, E & Marken, F 2018, 'One-step preparation of microporous Pd@cPIM composite catalyst film for triphasic electrocatalysis', *Electrochemistry Communications*, vol. 86, pp. 17-20. <https://doi.org/10.1016/j.elecom.2017.11.007>

DOI:

[10.1016/j.elecom.2017.11.007](https://doi.org/10.1016/j.elecom.2017.11.007)

Publication date:

2018

Document Version

Peer reviewed version

[Link to publication](#)

Publisher Rights

CC BY-NC-ND

University of Bath

Alternative formats

If you require this document in an alternative format, please contact:
openaccess@bath.ac.uk

General rights

Copyright and moral rights for the publications made accessible in the public portal are retained by the authors and/or other copyright owners and it is a condition of accessing publications that users recognise and abide by the legal requirements associated with these rights.

Take down policy

If you believe that this document breaches copyright please contact us providing details, and we will remove access to the work immediately and investigate your claim.

Revision

20th October 2017

One-Step Preparation of Microporous Pd@cPIM Composite Catalyst Film for Triphasic Electrocatalysis

Shi Xuan Leong,^{1,2} Mariolino Carta,³ Richard Malpass-Evans,³ Neil B. McKeown,³ Elena Madrid,¹ and Frank Marken*¹

¹ *Department of Chemistry, University of Bath, Bath BA2 7AY, UK*

² *Division of Chemistry & Biological Chemistry, School of Physical & Mathematical Sciences, Nanyang Technological University, 20 Nanyang Link, Singapore 637371*

³ *EAStChem School of Chemistry, University of Edinburgh, Joseph Black Building, David Brewster Rd., Edinburgh, Scotland EH9 3FJ, UK*

To be submitted to *Electrochemistry Communications*

Abstract

Triphasic microporous materials (containing solid, liquid, and gas) are of interest in electrocatalysis. In this exploratory study, a polymer of intrinsic microporosity (PIM-EA-TB) is impregnated with PdCl_4^{2-} metal precursor and vacuum-carbonised to give an electrically conductive microporous heterocarbon with embedded Pd nanoparticles of typically 10 - 30 nm diameter. This microporous composite catalyst is formed (*via* spin-coating) as “flakes” of typically 100 nm thickness and 1 to 20 μm diameter that are readily re-deposited onto glassy carbon electrode substrates. Due to triphasic conditions, Pd@cPIM electrocatalytic reactivity is high but only for gases (H_2 oxidation or O_2 reduction). This selectivity is observed even in the presence of excess formic acid fuel in the aqueous/liquid phase. Potential for application in membrane-less micro-fuel cells is discussed.

Keywords: gas binding; triple phase reaction zone; fuel cell; CO_2 reduction; microporosity.

1. Introduction

Multi-phasic systems are crucial in electrocatalysis where poorly soluble gases such as hydrogen, oxygen, carbon dioxide, or ammonia need to effectively interact with nano-catalysts in three dimensional catalyst architectures [1,2]. Enhancing reactivity is possible by increasing pressure or by employing triple-phase boundary gas | liquid | solid reactions conditions [3]. Enhancing reactivity in the triple phase boundary reaction zone is linked to microporosity, surface energy, and catalyst design.

Recently, novel materials have emerged with “triphasic” characteristics in metal-organic frameworks [4], clays [5], zeolites [6], and in porous carbons [7]. Perhaps surprisingly, the presence of the liquid sometimes serves to enhance the gas binding ability of the microporous material [8]. For an electrically conductive microporous carbon material with both gas and liquid electrolyte permeating through the pores it can be proposed that diffusion of gases is affected beneficially (*via* gas inclusions) and diffusion of aqueous solutes is affected detrimentally (blocked by gas inclusions).

Polymers of intrinsic microporosity (PIMs) [9]) are comprised of a continuous rigid network of inter-connected micropores, typically less than 2 nm in size. Due to the high structural rigidity of the polymer backbone, efficient packing is hindered and consequently PIMs possess a large number of void spaces for liquid and gas to permeate. Additionally, PIMs (such as PIM-EA-TB, prepared from a diaminoethanoanthracene “EA” monomer via a Tröger base “TB” coupling [10], see structure in Figure 1) are readily soluble in organic solvents (chloroform) and can be easily processed to give coatings and deposits. These highly microporous materials are predominantly being developed for membrane gas separations [11], but have also attracted attention for heterogeneous electrocatalysis [12].

In this study, the polymer PIM-EA-TB is converted into a microporous heterocarbon under mild carbonisation conditions at 500 °C. It was recently demonstrated that during vacuum-carbonisation of PIM-EA-TB a decrease in surface area occurs (the Brunauer-Emmett-Teller or BET surface area changed from 1027 m²g⁻¹ to 242 m²g⁻¹) but microporosity increased [13]. In related studies, a nano-particulate heterocarbon material with slow ingress of aqueous electrolyte and with pH-dependent capacitance was obtained [14] and nano-platinum was

formed embedded in the microporous heterocarbon [15]. Here, nano-palladium is embedded into carbonised PIM-EA-TB (or Pd@cPIM). There are previous reports on the formation and application in catalysis of nano-palladium embedded into heterocarbon host materials [16,17]. Here the nano-composite is prepared *via* one-step vacuum-carbonisation and tested for electrocatalytic properties.

2. Experimental

2.1. Materials and Reagents. Chemicals were purchased from Sigma-Aldrich and used without purification. PIM-EA-TB was obtained following a literature procedure [10]. Laboratory grade hydrogen gas, oxygen gas, and argon gas were obtained from BOC, UK. Solutions were prepared using deionised water (with resistivity of 18.2 M Ω cm at 22 °C).

2.2. Catalyst Preparation Conditions. PIM-EA-TB was dissolved in chloroform (4 weight %). Thin polymer films were prepared on glass microscopy cover slips by spin coating at a rotation speed of 1000 rpm for 1 minute (WS-650Mz-23NPP, Laurell Technologies), immersion in PdCl₄²⁻ precursor solution (10 mM PdCl₂ in 0.1 M HCl) for 5 minutes, and then rinsing and drying under ambient conditions to give an orange-yellow films. Vacuum carbonisation was performed for samples wrapped in aluminium foil and under oil pump vacuum (ca. 0.2 mbar) in a quartz tube at 500 °C for 3 h.

2.3. Electrode Preparation. Vacuum-carbonised samples (Pd@cPIM or cPIM, estimated 200-300 μ g per sample) were stripped from the glass cover slips by sonication/scraping of flakes into 1.5 cm³ isopropanol to form a suspension. A volumes of 12 μ L (with estimated 0.2 mg cm⁻³) was drop-cast onto glassy carbon (GC) electrodes and dried to yield a modified surface with

approximately of 1.6 – 2.4 μg of the material of interest. Electrochemical measurements were performed at room temperature with a Ivium Compactstat (Ivium, Netherlands) in three-electrode cells with KCl-saturated reference electrode, GC working electrode (BAS, 3 mm diameter), and Pt wire counter electrode. In some experiments a palladium foil $3 \times 3 \text{ mm}^2$ on a glass support served as the working electrode.

3. Results and Discussion

3.1. Characterisation of Pd@cPIM. Figures 1A and 1B show TEM data for Pd@cPIM and for cPIM. The electron diffraction pattern (Figure 1C) confirms the presence of Pd nanoparticles [18], which are typically 10 to 30 nm in diameter. SEM data suggest typical flake sizes of 1-20 μm with a thickness of about 0.1 μm (Figure 1D). As seen from the Raman data in Figure 1E, the main peak at 1354 cm^{-1} can be assigned to the D-peak of disordered amorphous carbon, while the 1598 cm^{-1} peak is attributed to the G-peak of graphitic carbon [19]. Consistent with previous work, further deconvolution of the Raman spectra gives a shoulder peak corresponding to the TPA-band as well as the A band [14].

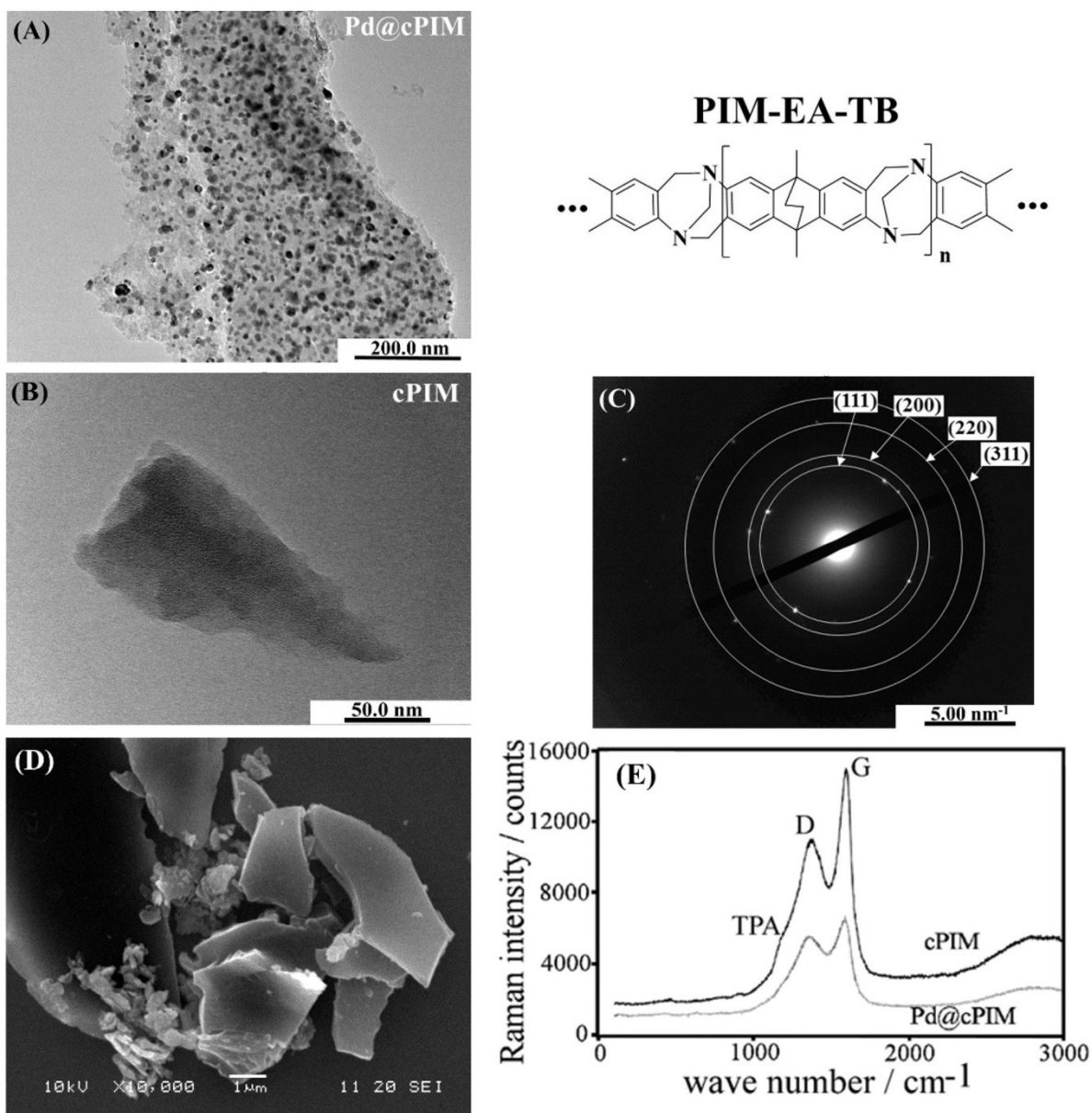


Figure 1. (A, B) TEM images for Pd@cPIM and cPIM flakes. (C) TEM diffraction pattern for embedded nano-palladium. (D) SEM images for cPIM flakes. (E) Raman data for cPIM and Pd@cPIM showing characteristic TPA shoulder and D- and G-bands for carbon.

3.2. Hydrogen Oxidation. Initially the electrocatalytic oxidation of H_2 (1 atm, in 0.1 M HClO_4 electrolyte at a scan rate of 10 mV s^{-1}) is employed to characterise the reactivity of the different electrode materials. Figure 2A shows absence of catalysis on bare GC but presence of H_2 oxidation (ca. $40 \mu\text{A cm}^{-2}$) on both bare Pd and Pd@cPIM. The high capacitive background current for Pd@cPIM is consistent with values reported for similar materials [14], but the lack

of observable Pd surface redox processes for Pd@cPIM suggests that a dense micro-porous heterocarbon has been formed when compared to recently reported Pt@cPIM materials [15].

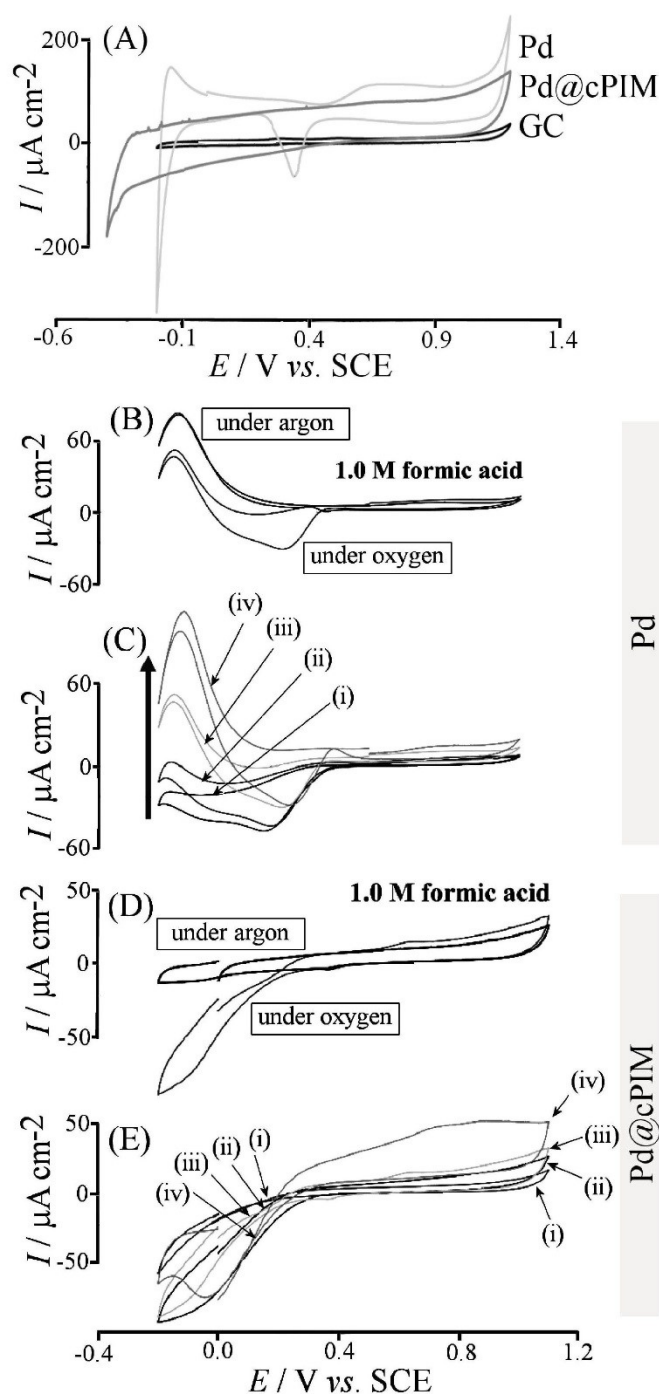


Figure 2. (A) CVs (scan rate 10 mV s^{-1}) for a GC electrode, bare Pd, and Pd@cPIM deposited on GC immersed in hydrogen-saturated 0.1 M HClO₄. (B, D) CVs (scan rate 1 mV s^{-1}) for a bare Pd and a Pd@cPIM-modified glassy carbon in 1.0 M HCOOH under argon or oxygen saturated conditions. (C, E) CVs (scan rate 1 mV s^{-1}) for a pure Pd and a Pd@cPIM-modified GC in oxygen-saturated HCOOH of varying concentrations at (i) 0.1 M, (ii) 0.5 M, (iii), 1.0 M and (iv) 5.0 M.

3.3. Oxygen Reduction in the Presence of Formic Acid. Figure 2B shows CVs for the oxidation of formic acid on bare Pd. Oxidation occurs at -0.2 V vs. SCE consistent with formic acid decomposition to adsorbed hydrogen and CO₂ [20,21]. The presence of oxygen is revealed by its onset at +0.3 V vs. SCE. The effects of varying formic acid concentration are shown (Figure 2B,C). Thus, on a bare Pd catalyst, two competing processes (oxygen reduction and formic acid oxidation) occur simultaneously. For Pd@cPIM (Figure 2D,E), the onset of oxygen reduction occurs again at approximately +0.3 V vs. SCE. No significant formic acid oxidation peak is recorded, suggesting that while Pd@cPIM is electrocatalytically reactive, activity is only limited to oxygen reduction. At high formic acid concentrations (5.0 M), the shape of the CV begins to change and formic acid oxidation seems likely but only at potentials positive of 0.3 V vs. SCE.

Next, a two-electrode system was investigated with both bare Pd and Pd@cPIM electrodes immersed in aqueous 1.0 M or 5.0 M formic acid (Figure 3A). The open circuit voltage is approximately 0.28 V for 1.0 M formic acid (and slightly less for 5.0 M formic acid). This is due to a negative potential at the bare Pd (where formic acid oxidation dominates) and a positive potential at the Pd@cPIM electrode (where oxygen reduction dominates). A voltage scan shows power generation in the potential range from 0.28 V to lower potentials. However, the curves do not retrace when scanning the potential back positive; some catalytic efficiency is lost in the high current region. The power plot (Figure 3B) shows a maximum power at approximately 0.15 V. Doubling the amount of Pd@cPIM catalyst can increase both voltage and power (Figure 3C). A power of 5 $\mu\text{W cm}^{-2}$ is reasonable when compared to similar membrane-less micro-fuel cell systems [22] and limited here mainly by the kinetically slow oxygen reduction reaction. There are previous reports of membrane-less formic acid fuel cells

being operated at higher temperature and higher power density with flow [21]. In order to improve the stationary micro-power generator more catalyst could be applied. The reaction of oxygen on bare Pd also needs to be suppressed (e.g. by reactor design exploiting the microporosity of Pd@cPIM in a gas diffusion electrode and keeping bare Pd as internal electrode).

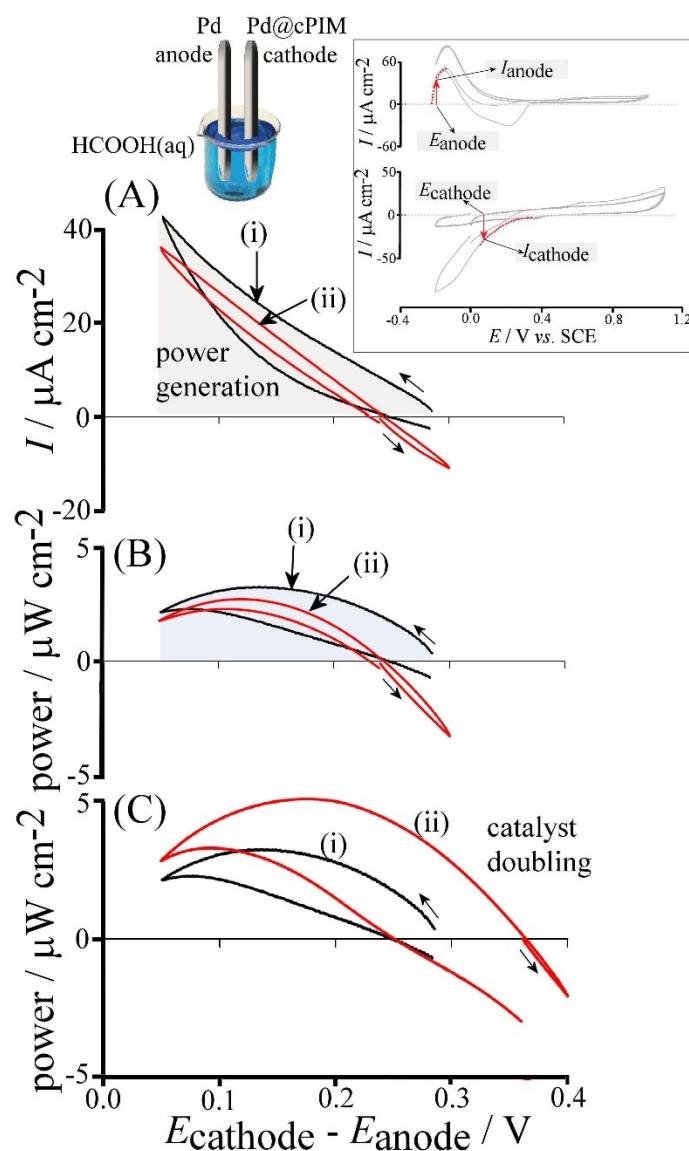


Figure 3. (A) Two-electrode voltammetry (scan rate 1 mV s^{-1}) for pure palladium (anode) and Pd@cPIM (cathode) immersed in (i) 1.0 M and (ii) 5.0 M formic acid (inset showing the parameters $E_{\text{cathode}} - E_{\text{anode}}$, I_{anode} , and I_{cathode} in voltammetry data). (B) Power (= current \times voltage) plotted versus voltage. (C) Power plotted for the two-electrode experiment in 1.0 M formic acid with (i) one deposition and (ii) two depositions of Pd@cPIM.

4. Conclusions

It has been shown that selectivity for gas phase reactions (hydrogen oxidation and oxygen reduction) can be achieved when embedding nano-Pd catalyst into a microporous heterocarbon host. Triphasic conditions are related to the chemical nature of the PIM precursor material and to the conditions during carbonisation. Further work will be needed to quantify the ratio of liquid to gas phase within the catalyst. There are many potential applications where effective and selective gas phase reactions are important including hydrogen, ammonia and methane fuel cells. Catalyst selectivity is also crucial for membrane-less micro-power generator applications.

Acknowledgements

SXL thanks Nanyang Technological University and the CN Yang Scholars Programme Office for support. EM, FM and NBM are grateful for support from the Leverhulme Foundation (RPG-2014-308).

References

-
- [1] H.J. Huang, X. Wang, Recent progress on carbon-based support materials for electrocatalysts of direct methanol fuel cells, *J. Mater. Chem. A* 2 (2014) 6266–6291.
 - [2] L. Zhang, Z.J. Zhao, J.L. Gong, Nanostructured materials for heterogeneous electrocatalytic CO₂ reduction and their related reaction mechanisms, *Angew. Chem. Internat. Ed.* 56 (2017) 11326–11353.
 - [3] F. Marken, J.D. Watkins, A.M. Collins, Ion-transfer- and photo-electrochemistry at liquid vertical bar liquid vertical bar solid electrode triple phase boundary junctions: perspectives, *Phys. Chem. Chem. Phys.* 13 (2011) 10036–10047.

-
- [4] G.A. Gonzalez-Martinez, J.A. Zarate, A. Martinez, E. Sanchez-Gonzalez, J.R. Alvarez, E. Lima, E. Gonzalez-Zamora, I.A. Ibarra, Confinement of alcohols to enhance CO₂ capture in MIL-53(Al), *RSC Adv.* 7 (2017) 24833–24840.
- [5] A. Kadoura, A.K. Narayanan Nair, S. Sun, Adsorption of carbon dioxide, methane, and their mixture by montmorillonite in the presence of water, *Microporous Mesoporous Mater.* 225 (2016) 331–341.
- [6] N.H. Linh, Y. Schuurman, D. Farrusseng, B. Coasne, Solubility of gases in water confined in nanoporous materials: ZSM-5, MCM-41, and MIL-100, *J. Phys. Chem. C* 119 (2015) 21547–21554.
- [7] P. Billemont, B. Coasne, G. De Weireld, Adsorption of carbon dioxide-methane mixtures in porous carbons: effect of surface chemistry, *Adsorption* 20 (2014) 453–463.
- [8] J.T. Wang, S.F. Wang, Q.P. Xin, Y.F. Li, Perspectives on water-facilitated CO₂ capture materials, *J. Mater. Chem. A* 5 (2017) 6794–6816.
- [9] N.B. McKeown, P.M. Budd, Exploitation of intrinsic microporosity in polymer-based materials, *Macromolecules* 43 (2010) 5163–5176.
- [10] M. Carta, R. Malpass-Evans, M. Croad, Y. Rogan, J.C. Jansen, P. Bernardo, F. Bazzarelli, N.B. McKeown, An efficient polymer molecular sieve for membrane gas separations, *Sci.* 339 (2013) 303–307.
- [11] M. Carta, M. Croad, R. Malpass-Evans, J.C. Jansen, P. Bernardo, G. Clarizia, K. Friess, M. Lanc, N.B. McKeown, Triptycene induced enhancement of membrane gas selectivity for microporous Träger's base polymers, *Adv. Mater.* 26 (2014) 3526–3531.
- [12] D.P. He, Y.Y. Rong, Z.K. Kou, S.C. Mu, T. Peng, R. Malpass-Evans, M. Carta, N.B. McKeown, F. Marken, Intrinsically microporous polymer slows down fuel cell catalyst corrosion, *Electrochem. Commun.* 59 (2015) 72–76.
- [13] Y.Y. Rong, D.P. He, A. Sanchez-Fernandez, C. Evans, K.J. Edler, R. Malpass-Evans, M. Carta, N.B. McKeown, T.J. Clarke, S.H. Taylor, A.J. Wain, J.M. Mitchels, F. Marken, Intrinsically microporous polymer retains porosity in vacuum thermolysis to electroactive heterocarbon, *Langmuir* 31 (2015) 12300–12306.
- [14] N. Hernandez, J. Iniesta, V.M. Leguey, A.R. Armstrong, S.H. Taylor, E. Madrid, Y.Y. Rong, R. Castaing, R. Malpass-Evans, M. Carta, N.B. Mckeown, F. Marken, Carbonization of polymers of intrinsic microporosity to microporous heterocarbon: capacitive pH measurements, *Appl. Mater. Today* 9 (2017) 136–144.
- [15] Y.Y. Rong, D.P. He, R. Malpass-Evans, M. Carta, N.B. McKeown, M.F. Gromboni, L.H. Mascaro, G.W. Nelson, J.S. Foord, P. Holdway, S.E.C. Dale, S. Bending, F. Marken,

High-utilisation nanoplatinum catalyst (Pt@cPIM) obtained via vacuum carbonisation in a molecularly rigid polymer of intrinsic microporosity, *Electrocatalysis*, 8 (2017) 132–143.

[16] X. Xu, Y. Li, Y.T. Gong, P.F. Zhang, H.R. Li, Y. Wang, Synthesis of palladium nanoparticles supported on mesoporous N-doped carbon and their catalytic ability for biofuel upgrade, *J. Amer. Chem. Soc.*, 134 (2012) 16987–16990.

[17] T. Harada, S. Ikeda, F. Hashimoto, T. Sakata, K. Ikeue, T. Torimoto, M. Matsumura, Catalytic activity and regeneration property of a Pd nanoparticle encapsulated in a hollow porous carbon sphere for aerobic alcohol oxidation, *Langmuir*, 26 (2010) 17720–17725.

[18] J.-G. Li, C.-Y. Tsai, S.-W. Kuo, Fabrication and characterization of inorganic silver and palladium nanostructures within hexagonal cylindrical channels of mesoporous carbon, *Polym.* 6 (2014) 1794–1802.

[19] A.C. Ferrari, Raman spectroscopy of graphene and graphite: disorder, electron–phonon coupling, doping and nonadiabatic effects, *Solid State Commun.* 143 (2007) 47–57.

[20] H. Meng, D.R. Zeng, F.Y. Xie, Recent development of Pd-based electrocatalysts for proton exchange membrane fuel cells, *Catalysts* 5 (2015) 1221–1274.

[21] L. An, R. Chen, Direct formate fuel cells: A review, *J. Power Sources* 320 (2016) 127–139.

[22] M.N. Nasharudin, S.K. Kamarudin, U.A. Hasran, M.S. Masdar, Mass transfer and performance of membrane-less micro fuel cell: A review, *Internat. J. Hydrogen Energy* 39 (2014) 1039–1055.